Fuzzy, ANN, and regression models to predict longitudinal dispersion coefficient in natural streams

Gokmen Tayfur

Department of Civil Engineering, Izmir Institute of Technology, Gulbahcekoyu, Urla, Izmir 35340, Turkey.
E-mail: *gokmentayfur@iyte.edu.tr*

Received 8 May 2005; accepted in revised form 26 January 2006

Abstract This study developed fuzzy, ANN, and regression-based models to predict longitudinal dispersion coefficient in natural streams from flow discharge data. 92 sets of field data were employed to calibrate and validate the models. 63 sets of data were used for the calibration while the remaining data were used for the validation of the models. The model-prediction results revealed the superiority of the developed models over the existing equations. The developed models predicted the measured data satisfactorily with minimum errors and maximum accuracy rates. The three models had comparable performances although the fuzzy model had the highest accuracy rate (79%) and lowest mean relative error (0.85).

Keywords ANN; calibration; dispersion coefficient; fuzzy; modeling; regression; validation

Introduction

Hazardous contaminants and effluent, when accidentally discharged into a river, undergo stages of mixing as they are transported downstream by the flowing water. The effluent is dispersed transversely, vertically, and longitudinally by advective and dispersive processes. Once the cross-sectional mixing is complete, the process of longitudinal dispersion becomes the most important mechanism (Seo and Cheong 1998). The intensity of the longitudinal dispersion is measured by the longitudinal dispersion coefficient (Deng *et al.* 2002). Hence, the transport process, and consequently the fate of the pollutants, depend, to a large extent, on the longitudinal dispersion coefficient. For that reason, this coefficient has been extensively investigated (Elder 1959; Sooky 1969; McQuivery and Keefer 1976; Sukhodolov *et al.* 1997). Taylor (1953, 1954) first introduced the longitudinal dispersion coefficient as a measure of the one-dimensional dispersion process and Fischer *et al.* (1979) developed the following integral expression for it:

$$K_x = \frac{1}{A}\int_0^B hu' \int_0^y \frac{1}{\varepsilon_t h}\int_0^y hu'\,dy\,\mathrm{d}y\,\mathrm{d}y \tag{1}$$

where K_x = longitudinal dispersion coefficient; A = cross-sectional area; B = channel width; h = local flow depth; u' = deviation of local depth mean flow velocity from cross-sectional mean; y = coordinate in the lateral direction; and ϵ_t = local transverse mixing coefficient.

By qualitative analysis and simplifications of Equation (1), and applying the one-step Huber method, Seo and Cheong (1998) obtained the following approximate formula for the longitudinal dispersion coefficient:

$$\frac{K_x}{Hu_*} = 5.915\left(\frac{B}{H}\right)^{0.62}\left(\frac{U}{u_*}\right)^{1.428} \tag{2}$$

Nordic Hydrology **Vol 37 No 2 pp 143–164** © IWA Publishing 2006

doi: 10.2166/nh.2006.005

where $H =$ cross-sectional average flow depth; $u^* =$ shear velocity; and $U =$ cross-sectional average flow velocity. The term on the left hand side of Equation (2) is called the dimensionless dispersion coefficient. Seo and Cheong (1998) showed that the accuracy of Equation (2) is higher than those of the previously developed and commonly employed six different equations in predicting the coefficient in natural streams.

Deng *et al.* (2001) developed a more theoretically based approximation of Equation (1). They first developed mathematical expressions for the lateral distribution of river flow depth (h), the deviation of the velocity from the mean flow velocity (u'), and the local transverse mixing coefficient (ϵ_t). Then, they incorporated these so-developed expressions into Equation (1) to obtain the following equation for predicting the dispersion coefficient:

$$\frac{K_x}{Hu_*} = \frac{0.15}{8\varepsilon_{to}}\left(\frac{B}{H}\right)^{5/3}\left(\frac{U}{u_*}\right)^2 \tag{3}$$

where

$$\varepsilon_{to} = 0.145 + \left(\frac{1}{3520.0}\right)\left(\frac{B}{H}\right)^{1.38}\left(\frac{U}{u_*}\right) \tag{4}$$

where ϵ_{to} is the dimensionless transverse mixing coefficient. The model of Deng *et al.* (2001) expressed by Equation (3) is more theoretically based. It not only includes the conventional parameters of the hydraulic variables (B/H), and the friction term (U/u_*) but also the effects of the transverse mixing (ϵ_{to}). Furthermore, it also, to a limited extent, considers the effects of non-uniformities. In their development, however, they made several assumptions. As a result, their model is, in theory, limited to straight-uniform streams whose width to depth ratio is greater than 10. Deng *et al.* (2001) showed that their model performs better than the model of Seo and Cheong (1998) in predicting the coefficient in natural streams.

Kashefipour and Falconer (2002) developed an equation for predicting the longitudinal dispersion coefficient in riverine flows using 81 sets of measured data from 30 rivers. This equation relates the dispersion coefficient to the hydraulic and geometric parameters and was derived by using dimensional and regression analyses, and can be expressed as

$$K_x = 10.612(HU)\left(\frac{U}{u_*}\right). \tag{5}$$

In the above equations K_x is expressed as a function of flow and channel characteristics parameters (U, u^*, H, B, B/H, U/u^*). The performance of these equations varies widely for the same stream and flow conditions. The measured field data obtained from Seo and Cheong (1998), Deng *et al.* (2001, 2002) and Kashefipour and Falconer (2002) are presented in Table 1. The scatter diagrams between the parameters and K_x are presented in Figure 1. The coefficient of determination (R^2) for each diagram is also shown on each graph. As can be seen, there is no strong dependence between each parameter and K_x. This fact was also discussed and demonstrated by Toprak *et al.* (2004) who generated the arithmetical and logarithmical scatter diagrams between the parameters and K_x using the field data from Kashefipour and Falconer (2002).

The desire to search for a better model is hence continued by Deng *et al.* (2002) who developed a theoretical model which has a general applicability for a wide range of field conditions. They showed the superiority of their model over the previously developed models. However, their model has a major drawback in terms of its complexity coming from an application of approximation methods for triple numerical integration with a set of regression equations (Rowinski *et al.* 2005). The following formulation is also used by Deng *et al.* (2002) and Rowinski *et al.* (2005) to predict the dispersion coefficient:

$$K_x = 3UB. \tag{6}$$

Table 1 Experimental measurements of channel characteristics, flow variables and longitudinal dispersion coefficient in natural streams (* Used for verifying the developed models–Equation (7), ANN, fuzzy)

No	Stream	B (m)	H (m)	U (m/s)	u^* (m/s)	B/H	U/u^*	β	σ	$3UB$ (m^2/s)	Q (m^3/s)	K_x (m^2/s)
1	Antietam Creek, MD	12.8	0.3	0.42	0.057	42.7	7.37	3.75	1.4	16.1	1.6	17.5
2	"	24.1	0.98	0.59	0.098	24.6	6.02	3.2	2.25	42.7	13.9	101.5
3	"	21	0.48	0.62	0.069	43.8	8.99	3.78	1.26	39.1	6.2	25.9
4	"*	11.9	0.66	0.43	0.085	18	5.06	2.89	2.25	15.4	3.4	20.9
5	Monocacy River, MD*	48.7	0.55	0.26	0.052	88.5	5	4.48	1.28	38.0	7.0	37.8
6	"*	93	0.71	0.16	0.046	131	3.48	4.88	1.28	44.6	10.6	41.4
7	"	51.2	0.65	0.62	0.044	78.8	14.09	4.37	1.28	95.2	20.6	29.6
8	"	97.5	1.15	0.32	0.058	84.8	5.52	4.44	1.61	93.6	35.9	119.8
9	"	40.5	0.41	0.23	0.04	98.8	5.75	4.59	1.61	27.9	3.8	66.5
10	Conococheague Creek, MD	42.2	0.69	0.23	0.064	61.2	3.59	4.11	2.25	29.1	6.7	40.8
11	"*	43	1.13	0.63	0.081	38.1	7.78	3.64	1.31	81.3	30.6	53.3
12	"	49.7	0.41	0.15	0.081	121.2	1.85	4.8	2.25	22.4	3.1	29.3
13	Chattahoochee River, GA*	75.6	1.95	0.74	0.138	38.8	5.36	3.66	1.27	167.8	109.1	88.9
14	"*	91.9	2.44	0.52	0.094	37.7	5.53	3.63	1.57	143.4	116.6	166.9
15	Salt Creek, NE	32	0.5	0.24	0.038	64	6.32	4.16	1.38	23.0	3.8	52.2
16	Diffcult Run, VA	14.5	0.31	0.25	0.062	46.8	4.03	3.85	1.09	10.9	1.1	1.9
17	Bear Creek, CO*	13.7	0.85	1.29	0.553	16.1	2.33	2.78	1.08	53.0	15.0	2.9
18	Little Pincy Creek, MD	15.9	0.22	0.39	0.053	72.3	7.36	4.28	1.13	18.6	1.4	7.1
19	Bayou Anacoco, LA	17.5	0.45	0.32	0.024	38.9	13.33	3.66	1.41	16.8	2.5	5.8
20	"	25.9	0.94	0.34	0.067	27.6	5.07	3.32	1.41	26.4	8.3	32.5
21	"	36.6	0.91	0.4	0.067	40.2	5.97	3.69	1.41	43.9	13.3	39.5
22	Comite River, LA	15.7	0.23	0.36	0.039	68.3	9.23	4.22	1.31	17.0	1.3	69
23	Bayou Barthol. LA	33.4	1.4	0.2	0.031	23.9	6.45	3.17	2.46	20.0	9.4	54.7
24	Tickfau River, LA	15	0.59	0.27	0.08	25.4	3.38	3.23	1.75	12.2	2.4	10.3
25	Tangipahoa River, LA	31.4	0.81	0.48	0.072	38.8	6.67	3.66	1.46	45.2	12.2	45.1
26	"*	29.9	0.4	0.34	0.02	74.8	17	4.31	1.46	30.5	4.1	44
27	Red River, LA	253.6	1.62	0.61	0.032	156.5	19.06	5.05	1.2	464.1	250.6	143.8
28	"*	161.5	3.96	0.29	0.06	40.8	4.83	3.93	1.44	140.5	185.5	130.5

Table 1 – *continued*

No	Stream	B (m)	H (m)	U (m/s)	u^* (m/s)	B/H	U/u^*	β	σ	$3UB$ (m^2/s)	Q (m^3/s)	K_x (m^2/s)
29	“*	152.4	3.66	0.45	0.057	41.6	7.89	3.73	1.44	205.7	251.0	227.6
30	“	155.1	1.74	0.47	0.036	89.1	13.06	4.49	1.24	218.7	126.8	177.7
31	Sabina River, LA	116.4	1.65	0.58	0.054	70.5	10.74	4.26	1.19	202.5	111.4	131.3
32	“*	160.3	2.32	1.06	0.054	69.1	19.63	4.24	1.17	509.8	394.2	308.9
33	Sabina River, TX*	14.2	0.5	0.13	0.037	28.4	3.51	3.35	2.53	5.5	0.9	12.8
34	“	12.2	0.51	0.23	0.03	23.9	7.67	3.17	2.05	8.4	1.4	14.7
35	“	21.3	0.93	0.36	0.035	22.9	10.29	3.13	1.47	23.0	7.1	24.2
36	Wind/Big. River, WY	44.2	1.37	0.99	0.142	32.3	6.97	3.48	1.56	131.3	59.9	184.6
37	“	85.3	2.38	1.74	0.153	35.8	11.37	3.58	1.56	445.3	353.2	464.6
38	“*	59.4	1.1	0.88	0.119	54	7.39	3.99	1.18	156.8	57.5	41.8
39	“	68.6	2.16	1.55	0.168	31.8	9.23	3.46	1.18	319.0	229.7	162.6
40	Copper Creek, VA	16.7	0.49	0.2	0.08	34.1	2.5	3.53	2.54	10.0	1.6	16.8
41	Powell River, TN*	33.8	0.85	0.16	0.055	39.8	2.9	3.68	–	16.2	4.6	9.5
42	Clinch River, VA*	36	0.58	0.3	0.049	62.1	6.1	4.13	–	32.4	6.3	8.08
43	Clinch River, VA	48.5	1.16	0.21	0.069	41.8	3.04	3.73	1.25	30.6	11.8	14.8
44	“*	28.7	0.61	0.35	0.069	47	5.07	3.85	1.14	30.1	6.1	10.7
45	“	57.9	2.45	0.75	0.104	23.6	7.21	3.16	1.14	130.3	106.4	40.5
46	“*	53.2	2.41	0.66	0.107	22.1	6.17	3.1	1.14	105.3	84.6	36.9
47	Copper Creek, VA	18.3	0.38	0.15	0.116	48.2	1.29	3.88	2.54	8.2	1.0	20.7
48	“	16.8	0.47	0.24	0.08	35.7	3	3.58	2.54	12.1	1.9	24.6
49	Powell River, TN*	36.8	0.87	0.13	0.054	42.3	2.41	3.74	2.2	14.4	4.2	15.5
50	Copper River, VA	19.6	0.84	0.49	0.101	23.3	4.85	3.15	1.26	28.8	8.1	20.8
51	Nooksack River, WA	64	0.76	0.67	0.268	84.2	2.5	4.43	1.3	128.6	32.6	34.8
52	John Day River, OR*	25	0.58	1.01	0.14	43.1	7.21	3.76	1.08	75.8	14.6	13.9
53	“*	34.1	2.47	0.82	0.18	13.8	4.56	2.62	1.89	83.9	69.1	65
54	Yadkin River, NC	70.1	2.35	0.43	0.101	29.8	4.26	3.39	2.17	90.4	70.8	111.5
55	“*	71.6	3.84	0.76	0.128	18.6	5.94	2.92	2.17	163.2	209.0	260.1
56	Minnesota River	80	2.74	0.034	0.0024	29.2	14.17	3.37	–	8.2	7.5	22.3
57	“	80	2.74	0.14	0.0097	29.2	14.43	3.37	–	33.6	30.7	34.9

Table 1 – *continued*

No	Stream	B (m)	H (m)	U (m/s)	u^* (m/s)	B/H	U/u^*	β	σ	$3UB$ (m^2/s)	Q (m^3/s)	K_x (m^2/s)
58	Amita River	37	0.81	0.29	0.07	45.7	4.14	3.82	–	32.2	8.7	23.2
59	“	42	0.8	0.42	0.069	52.5	6.09	3.96	–	52.9	14.1	30.2
60	White River*	67	0.59	0.35	0.044	113.6	7.95	4.73	–	70.4	13.8	30.2
61	Nooksack River	86	2.93	1.2	0.53	29.4	2.26	3.38	1.3	309.6	302.4	153
62	Susquehanna River	203	1.35	0.39	0.065	150.4	6	5.01	1.13	237.5	106.9	92.9
63	Bayou Anacoco	20	0.42	0.29	0.045	47.6	6.44	3.86	1.41	17.4	2.4	13.9
64	Muddy River	13	0.81	0.37	0.081	16	4.57	2.77	–	14.4	3.9	13.9
65	“	20	1.2	0.45	0.099	16.7	4.55	2.82	–	27.0	10.8	32.5
66	Comite River	13	0.26	0.31	0.044	50	7.05	3.91	1.31	12.1	1.0	7
67	“	16	0.43	0.37	0.056	37.2	6.61	3.62	1.31	17.8	2.5	13.9
68	Missouri River	183	2.33	0.89	0.066	78.5	13.48	4.36	1.35	488.6	379.5	465
69	“	201	3.56	1.28	0.084	56.5	15.24	4.03	1.35	771.8	915.9	837
70	“*	197	3.11	1.53	0.078	63.3	19.62	4.15	1.35	904.2	937.4	892
71	Copper Creek, VA*	15.9	0.49	0.21	0.079	32.4	2.7	3.48	–	10.0	1.6	19.5
72	“	18.3	0.84	0.52	0.1	21.8	5.2	3.08	–	28.5	8.0	21.4
73	“	16.2	0.49	0.25	0.079	33.1	3.2	3.50	–	12.2	2.0	9.5
74	Clinc River, TN	46.9	0.86	0.28	0.067	54.5	4.2	4.00	–	39.4	11.3	13.9
75	“*	53.3	2.09	0.79	0.107	25.5	7.4	3.24	–	126.3	88.0	46.5
76	“	59.4	2.13	0.86	0.104	27.9	8.3	3.33	–	153.3	108.8	53.9
77	Copper Crick, VA	18.6	0.39	0.14	0.116	47.7	1.2	3.86	–	7.8	1.0	9.9
78	Coachell Canal, CA	24.4	1.56	0.67	0.043	15.6	15.6	2.75	–	49.0	25.5	9.6
79	Antietam Creek	15.8	0.39	0.32	0.06	40.5	5.3	3.70	–	15.2	2.0	9.3
80	“*	19.8	0.52	0.43	0.069	38.1	6.2	3.64	–	25.5	4.4	16.3
81	“	24.4	0.71	0.52	0.081	34.4	6.4	3.54	–	38.1	9.0	25.6
82	Monocacy River	35.1	0.32	0.21	0.043	109.7	4.9	4.70	–	22.1	2.4	4.7
83	“*	36.6	0.45	0.32	0.051	81.3	6.3	4.40	–	35.1	5.3	13.9
84	“	47.5	0.87	0.44	0.07	54.6	6.3	4.00	–	62.7	18.2	37.2
85	Elkhorn River	32.6	0.3	0.43	0.046	108.7	9.3	4.69	–	42.1	4.2	9.3
86	“*	50.9	0.42	0.46	0.046	121.2	10.0	4.80	–	70.2	9.8	20.9

Table 1 – *continued*

No	Stream	B (m)	H (m)	U (m/s)	u^* (m/s)	B/H	U/u^*	β	σ	$3UB$ (m^2/s)	Q (m^3/s)	K_x (m^2/s)
87	Sabine River	103.6	2.04	0.56	0.054	50.8	10.4	3.93	–	174.0	118.4	315.9
88	Muddy Creek	13.4	0.81	0.37	0.077	16.5	4.8	2.80	–	14.9	4.0	13.9
89	“*	19.5	1.2	0.45	0.093	16.3	4.8	2.79	–	26.3	10.5	32.5
90	Sabine River, TX	35.1	0.98	0.21	0.041	35.8	5.1	3.58	–	22.1	7.2	39.5
91	Chattahoochee River	65.5	1.13	0.39	0.075	58.0	5.2	4.06	–	76.6	28.9	32.5
92	Bayou Anacoco, LA	17.5	0.45	0.32	0.024	38.9	13.3	3.66	–	16.8	2.5	5.8
Mean value		**53.79**	**1.18**	**0.49**	**0.083**	**50.3**	**7.1**	**3.76**	**1.55**		**68.7**	**79.98**
Standard deviation		34.2	0.69	0.26	0.075	19.4	2.83	0.37	0.29		109.1	102.3
X_{min}		11.9	0.23	0.034	0.0024	13.8	1.2	2.62	1.08		0.9	1.9
X_{max}		253.6	3.96	1.74	0.268	156.5	19.62	5.05	2.54		937.4	892

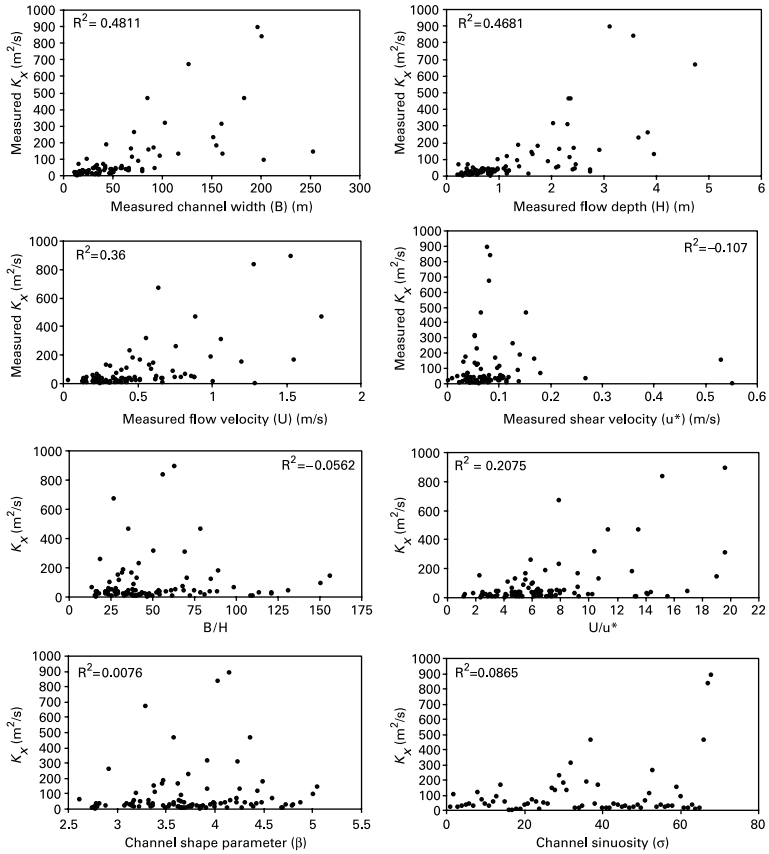

Figure 1 Scatter diagrams between parameters (B, H, U, u_*, B/H, U/u_*, β, σ, K_x)

Figure 2(a) shows the scatter diagram between ($3UB$) and K_x for the data presented in Table 1. As seen, there is a dependence between the two variables with $R^2 = 0.78$. This result implies the plausibility of the formulation. Note that the factor value of 3 in Equation (6) is not universal. In other studies different values were obtained. For example, Rochusaar and Paal (1970) obtained a value of 1.5 for small Estonian rivers, while Sukhodolov *et al.* (1997) obtained a value of 0.83 for the experimental results for Moldovian rivers. As such, the literature suggests, to me, that the value of the factor in Equation (6) might be related to the flow depth.

This study hence investigates whether the longitudinal dispersion coefficient may be predicted as a function of flow discharge. Figure 2(b) presents the scatter diagram between the $Q(= UHB)$ and K_x for the data in Table 1. As seen, there is a stronger dependence between the Q and K_x with $R^2 = 0.88$. As such, the following equation is proposed for predicting the longitudinal dispersion coefficient in natural streams:

$$K_x = \alpha Q + \varepsilon \tag{7}$$

where α and ϵ are model parameters that can be, as is presented later, obtained through the calibration procedure.

In addition to Equation (7), this study also proposes artificial intelligence methods of neural networks and fuzzy logic algorithms that would have general applicability to predict K_x from flow discharge. Rowinski *et al.* (2005) and Tayfur and Singh (2005) applied ANNs to predict K_x using (B/H), (U/u_*), ($3UB$) and (σ) (channel sinuosity) in the input vector of the

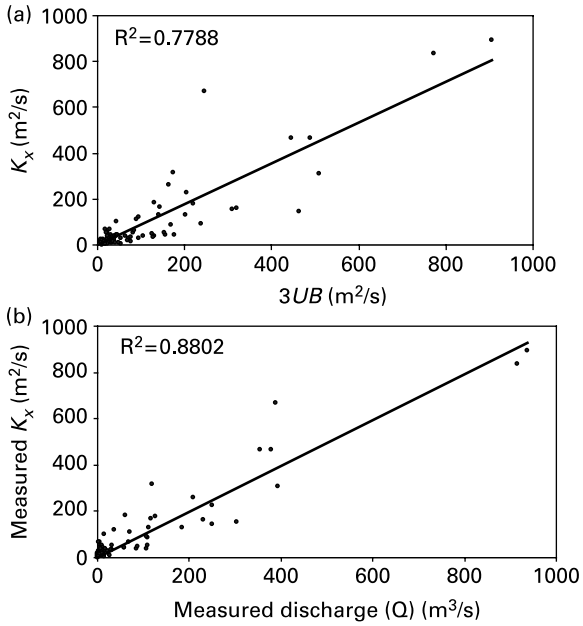

Figure 2 Scatter diagrams: (a) ($3UB$) and K_x; (b) Q and K_x

network. Although Rowinski *et al.* (2005) and Tayfur and Singh (2005) state that inclusion of σ in the input vector of the network improves prediction capability of the ANN, the scatter diagrams in Figure 1 show that there is, in essence, not a strong dependence between this parameter and K_x. Also, there is no dependence between channel shaper parameter (β) and K_x (Figure 1). Hence, this study, alternatively, develops ANN to predict K_x using Q in the input vector. ANNs have an ability to capture relationships from given patterns and this ability has enabled them to be employed in the solution of large-scale complex problems. However, ANNs are black box models that do not reveal any physical relations between the input and the output variables of the system. Hence it is difficult to have a good insight of the physical process. Thus, this study also develops a fuzzy logic model to predict K_x using Q in the input vector. Fuzzy model, unlike ANNs, might reveal insights into the understanding of the physical process through the fuzzy rules expressed in terms of IF–THEN statements. In addition, a fuzzy algorithm is well suited for handling vague data, as is the case in the dispersion process where there are imprecisions in both discrete measurements and parameter uncertainty over space and time.

The main purpose of this study is to develop fuzzy, ANN, and regression-based models to predict the dispersion coefficient in natural streams using flow discharge data in the input vector. These models can be alternatives to the existing empirical and theoretical equations. The performances of these models are quantitatively investigated.

Overview of fuzzy logic algorithm

The fuzzy approach has found wide application in the solution of hydrological processes (Dou *et al.* 1997, 1999; Raj and Kumar 1998; Chuntian, 1999; Abebe *et al.* 2000; Hundecha *et al.* 2001; Ozelkan and Duckstein 2001; Lu and Lo, 2002; Coppala *et al.* 2002; Tayfur *et al.* 2003; Sen and Altunkaynak 2003).

A general fuzzy system has basically four components—fuzzification, fuzzy rule base, fuzzy output engine, and defuzzification. *Fuzzification* converts each piece of input data to

degrees of membership. Fuzzy membership functions may take many forms, but in practical applications triangular ones are preferable (Sen 1998). *Fuzzy rule base* contains rules that include all possible fuzzy relations between inputs and outputs. These rules are expressed in the IF–THEN format. In the Sugeno rule system, the consequent part of the fuzzy rule is expressed as a mathematical function of the input variable. In the Mamdani rule system the consequent part is, however, expressed as a verbal statement (Jantzen 1999). *Fuzzy inference engine* takes into account all the fuzzy rules in the fuzzy rule base and learns how to transform a set of inputs to corresponding outputs. There are basically two subprocesses—inferencing and composition. In the inferencing subprocess, the truth value of each rule is computed and then applied to the consequent part of each rule. This results in one fuzzy subset to be assigned to each output variable for each rule. There are basically, for this purpose, two inferencing methods—minimization (min) and production (prod). In the composition subprocess all the fuzzy subsets assigned to each output variable are combined together to form a single subset for each output variable. There are basically, for this purpose, two composition methods—maximization (max) and summation (sum). The *defuzzification engine* converts the resulting combined output fuzzy subset to a crisp value. The center of gravity method is the most commonly used defuzzification method. In general, given a fuzzy set with membership degree $\mu(x)$ defined on the interval $[a, b]$ of variable x, the center of gravity defuzzification prediction, $\hat{x}$, is defined as (Sen and Altunkaynak 2003)

$$\hat{x} = \frac{\int_a^b x\mu(x)\mathrm{d}x}{\int_a^b \mu(x)\mathrm{d}x} \tag{8}$$

where $\hat{x} =$ defuzzified output value, $x_i =$ output value in the ith subset, and $\mu(x_i) =$ membership value of the output value in the ith subset. For the discrete case, the integrals in Equation (8) are replaced by summations.

The details of the fuzzy logic-based algorithm can be obtained from the literature (Zadeh and Kacprzyk 1992; Kosko 1992; McNeill and Thro 1994; Jantzen 1999; Sen 1999; Sen and Altunkaynak 2003).

Experimental data

This study employed 92 sets of measured data (Table 1). The data sets are obtained from Seo and Cheong (1998), Deng *et al.* (2001, 2002) and Kashefipour and Falconer (2002). In Table 1, σ is the channel sinuosity and it is defined as the ratio of the channel length to the valley length (Chang 1988). σ can be calculated from 1:25 000 scale topographic maps based on specific stream reaches of the dye tests (Deng *et al.* 2002). For straight channels, the sinuosity is equal to unity. In Table 1, β represents the channel shape parameter and is defined as $\beta = \ln(B/H)$ (Deng *et al.* 2001). If β is equal to 1.0 then the channel has a triangular shape. Otherwise, it would have either a parabolic shape ($\beta = 2$) or a channel shape with a flatbed region and two curving bank regions ($2 < \beta < 5$) or a rectangular shape ($\beta > 5$).

The range for the width-to-depth ratio (B/H) of the streams varies from 13.8 (almost narrow) to 156.5 (very wide). As such, there is no stream whose width-to-depth ratio (B/H) is less than 10. The channel shape parameter (β) varies from 2.62 to 5.05. According to Deng *et al.* (2001), this range corresponds to a natural channel shape with a flatbed region and two curving bank regions. The sinuosity (σ) of the streams and rivers varies from 1.08 (almost straight) to 2.54 (very sinusoidal). For a straight channel, the sinuosity is equal to unity. As seen in Table 1, most of the streams are sinusoidal.

Table 1 also summarizes the statistics (mean, standard deviation, minimum and maximum) for each variable. The data sets in Table 1 were separated into two groups as

calibration and validation sets. The validation set is marked by * in Table 1. The calibration set was used for developing and calibrating the models while the other set was used for verifying the developed models.

Regression-based model

As presented in Figure 2, there is a strong dependence between flow discharge (Q) and the longitudinal dispersion coefficient (K_x) with $R^2 = 0.88$. In order to obtain the parameter values of α and ϵ in Equation (7), 63 data sets (calibration set) were chosen from Table 1. The remaining 29 sets marked as * in Table 1 (validation set) were used for verifying the model. Note that the same sets were also employed for calibrating and validating the ANN and fuzzy models. Although the data for the calibration and validation sets were chosen randomly, special attention was paid so that the statistics of the sets would have the same magnitude of order. Such a precaution would avoid the bias in the model predictions. Table 2 summarizes the statistics for both the sets. As seen in Table 2, the statistics are of the same magnitude of order. In addition, extra attention was further paid to have representative data sets from different rivers in both the sets (Table 1).

When a linear regression line is fitted to the 63 calibration Q–K_x data sets as shown in Figure 3(a), it produces the following equation:

$$K_x = 0.906Q + 21.416. \tag{9}$$

As such, $\alpha = 0.906$ and $\epsilon = 21.416$ are obtained for this particular data set.

In order to investigate the appropriateness of Equation (9) (regression equation), it is first applied to predict the measured K_x values for the calibration set. Figure 3(b) presents the measured K_x versus Equation (9) predicted K_x values for the calibration set. For this calibration run $R^2 = 0.87$ and $MAE = 27.0\,\mathrm{m^2/s}$ (where R^2 is the "coefficient of determination" and MAE stands for the "mean absolute error"). Figure 3(b) also shows a band width with (where SE is the standard error) about the regression line, where the computed SE is $47.5\,\mathrm{m^2/s}$. As seen in Figure 3(b), there are only 4 points (out of 63) outside the band width. In other words, band width accounts for about 94% of the scatter points. These results imply the successful calibration of the model.

The calibrated model was then applied to predict the remaining 29 K_x values (validation set). Figure 3(c) presents the Equation (9)-predicted K_x versus measured K_x for the validation set. As seen, the model successfully predicted the measured data with $R^2 = 0.97$, $MRE = 0.97$ (where MRE is the mean relative error) and $MAE = 23.1\,\mathrm{m^2/s}$. Figure 3(c) also shows the band width about the regression line, where the computed SE is $29.8\,\mathrm{m^2/s}$. As seen in Figure 3(c), there is no point outside the band width. In other words, band width accounts for almost 100% of the scatter points. This implies that the developed regression-based model can predict about 100% of the measured data with $\mp 59.6\,\mathrm{m^2/s}$.

Table 2 Statistics for calibration and verification data sets

	Q ($\mathrm{m^3/s}$)				K_x ($\mathrm{m^2/s}$)			
	mean	st. dev.	min	max	mean	st. dev.	min	max
Calibration set	58.1	137.7	1.0	915.9	74.4	132.5	1.90	837.0
Verification set	91.5	184.1	0.90	937.4	92.4	170.5	2.90	892.0

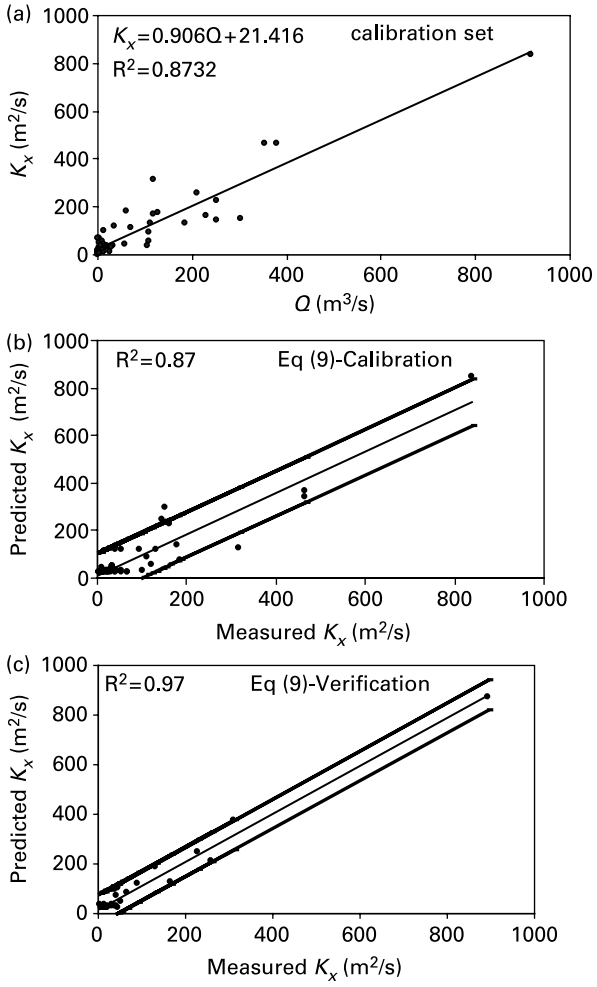

Figure 3 (a) Measured Q versus measured K_x for the calibration data set; measured K_x versus Equation (9)-predicted K_x; (b) calibration; (c) verification

Artificial neural network model

This study constructed a three-layer feed-forward ANN model. The model considered Q as the input variable and K_x as the output variable. The model employed the sigmoid function as the activation function and the back-propagation as the network training.

The constructed ANN model was first trained with the calibration set (Table 1). Figure 4(a) shows the calibration run. For this calibration run, the constructed ANN model employed 3 neurons in the hidden layer, 0.01 learning rate, 0.04 momentum factor, 9000 iterations, 0.1–0.6 as the initial random values for the connection weights, and -1.0 as the initial random value for the bias nodes. Also, all the external input and output values, before passing them into a neural network, were compressed into the range of [0.1–0.9]. The number of neurons in the hidden layer was decided by the commonly employed trial and error procedure. For this purpose the mean error (*ME*) and mean relative error (*MRE*) were used as error measures. Accordingly, the number of iterations that provided the minimum *ME* and *MRE* values was the stopping criterion for terminating the iterations. The values of these error measures started with $ME = 317.6\ \mathrm{m^2/s}$ and $MRE = 70.2$ at the first iteration and rapidly decreased to $62.6\ \mathrm{m^2/s}$ and 30.6, respectively after the 70th iteration. The errors then gradually decreased to and

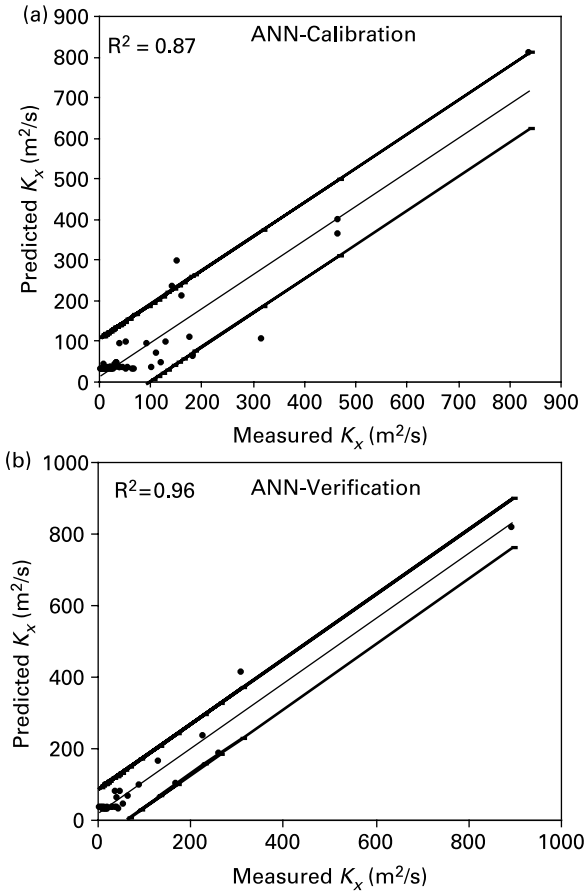

Figure 4 Measured K_x versus ANN-predicted K_x: (a) calibration run; (b) verification run

stabilized at $ME = 24.8\,m^2/s$ and $MRE = 14.5$ after 9000 iterations. The modeling details of ANNs are given elsewhere (ASCE 2000; Tayfur 2002; Rowinski *et al.* 2005; Tayfur *et al.* 2005; Tayfur and Singh 2005). The calibration run (Figure 4(a)) resulted in $R^2 = 0.87$ and $MAE = 30.4\,m^2/s$. Figure 4(a) also shows a band width with $\mp 2SE$ about the regression line, where the computed SE is $47.5\,m^2/s$. As seen in Figure 4(a), there are only 3 points (out of 63) outside the band width. In other words, band width accounts for about 95% of the scatter points. These results imply the successful calibration of the ANN model.

The trained (calibrated) ANN model was then applied to predict the remaining validation data set (marked by * in Table 1). Figure 4(b) presents the ANN validation run. As can be seen the model successfully predicted the measured data with $R^2 = 0.96$, $MAE = 25.7\,m^2/s$, and $MRE = 1.14$. Figure 4(b) also shows the band width about the regression line, where the computed SE is $35.4\,m^2/s$. As seen in Figure 4(b), there is only 1 point (out of 29) outside the band width. In other words, band width accounts for 97% of the scatter points. This implies that the developed ANN model can predict about 97% of the measured data with $\mp 70.8 m^2/s$.

Fuzzy model

As presented above, the regression-based model (Equation (9)) and ANN predicted K_x successfully using the flow discharge (Q) data. As such, the fuzzy model developed in this study considered Q as the input variable and K_x as the output variable. The commonly used triangular membership functions were employed for each fuzzy subset of each variable.

The number of fuzzy subsets for each variable is deduced from the data distribution of each variable. Note that the calibration set (63 data sets in Table 1) that is used to construct the regression-based model (Equation (9)) and the ANN model was also employed for constructing the fuzzy model. Figure 5(a) shows the data distribution for Q for the calibration set. As seen in Figure 5(a), the data clusters have centers around 20, 60, 120, 220 and 350 m^3/s. As such, as presented in Figures 6(a), 7 subsets—*very very low, very low, low, medium, high, very high, very very high*—were constructed. Note that the additional 2 subsets (*very very low* and *very very high*) are for the extreme low and extreme high values of the discharge. As such, $Q = 0$, 20, 60, 120, 220, 350, and 1000 m^3/s have the membership degree of 1.0 (Figure 6(a)). Figure 5(b) shows the data distribution for K_x for the calibration set. As seen in Figure 5(b), the data clusters have obvious centers around 30, 60, 140 and 260 m^2/s. As such, as presented in Figure 6(b), 7 subsets were constructed. 3 additional subsets (*very very low, very high, very very high*) were for the extreme low and extreme high values. Hence, according to Figure 6(b), 0, 30, 60, 140, 260, 500, and 1000 m^2/s have membership degree of 1.0.

Next, fuzzy rules relating Q to K_x were constructed from the calibration data set following the rule-construction-procedure given in the literature (Bardossy and Dissi 1993; Bardossy and Duckstein 1995; Ozelkan *et al.* 1996; Sen 1998; Coppala *et al.* 2002). This study employed the commonly used Mamdani rule system. The fuzzy rules were generated as follows. First, for a given data point (Q (i), $Kx(i)$; $i = 1,\ldots,N$; where N is the number of observations in the calibration set that is equal to 63) the memberships corresponding to the fuzzy regions are determined. Second, the data point to the fuzzy sets with the maximum membership value is assigned. The input–output data thus yields a rule. For example, in Figure 6(a), $Q = 111.4\ m^3/s$ belongs to the *low* set with membership $\mu_L = 0.20$ and to the *medium* set with membership $\mu_M = 0.80$. Similarly, the consequence $K_x = 131.3\ m^2/s$ belongs to the *low* set with membership $\mu_L = 0.10$ and to the *medium* set with membership $\mu_M = 0.90$. Then, (Q, Kx) would be assigned to "*medium*, *medium*" respectively and the following fuzzy rule would be obtained:

IF *Q is medium* ***THEN*** K_x *is medium* (10)

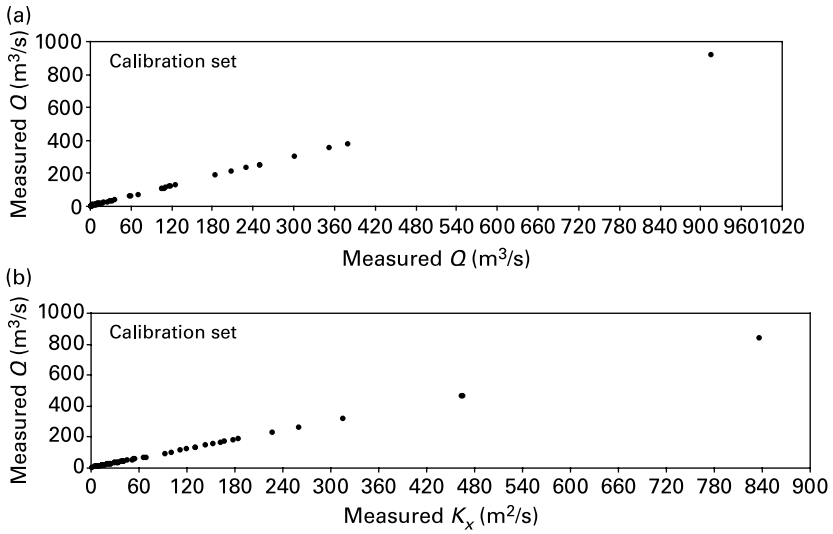

Figure 5 Measured data distribution: (a) flow discharge; (b) dispersion coefficient

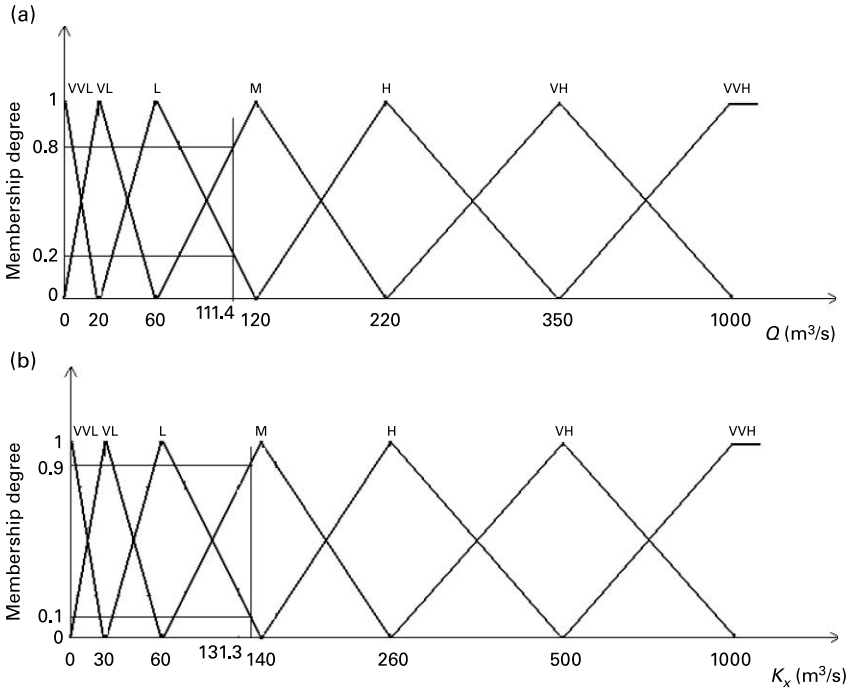

Figure 6 Fuzzy subsets: (a) flow discharge; (b) longitudinal dispersion coefficient (*V*: very; *L*: low; *M*: medium; *H*: high)

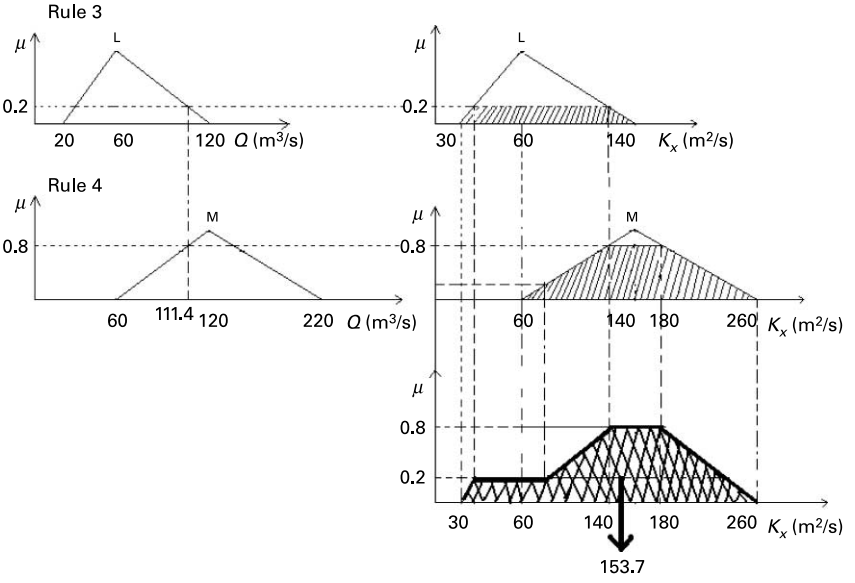

Figure 7 Fuzzy inferencing procedure and max composition

The weight of this rule is equal to $0.80 \times 0.90 = 0.72$. If this rule is not previously encountered, it is added to the rule bank, which will be used later for prediction purposes. This procedure is repeated for each input–output data pair. Note that it is sometimes possible to obtain the same rule with different weight. In that case, the rule with maximum weight is chosen. Also, it is possible to obtain more than one rule having the same propositional part (the first part of the rule that expresses the input fuzzy set, e.g. "**IF** Q is *medium*") but

a different consequent part (the last part of the rule that expresses the corresponding fuzzy output set, e.g. "**THEN** K_x is *medium*"). In such a case, the most frequently occurring rule that has the maximum weight is chosen. Through this procedure a total of 7 rules were constructed and they are presented in Table 3. As seen, the rules reflect almost the linear relation between Q and K_x agreeing with the regression-based model Equation (9) and Figure 2.

In order to show the application of fuzzy inference, in Figure 7 two rules of Q–K_x relationship are shown with membership degree, μ. Given $Q = 111.4\,\mathrm{m}^3/\mathrm{s}$ both *low* and *medium* fuzzy subsets of flow discharge are triggered. The consequent part of each K_x variable appears as a truncated trapezium for each rule on the right hand side in Figure 7. The overlapping of these two truncated trapeziums indicates the combined inference from these two rules in the lower part of the same figure which is represented in Figure 8 with relevant numbers. Note that the combined inference set is obtained using the max composition. In Figure 8 A1, A2, A3, A4, A5 and A6 indicate triangular and rectangular subareas in the fuzzy inference.

The final process in the fuzzy algorithm is the application of the defuzzification method to deduce a single value (crisp output value) from the combined fuzzy inference set. Applying the centroid defuzzification method expressed by Equation (8) to the combined inference set in Figure 8, it is possible to obtain a crisp output value (defuzzification value) by numerical calculation (Sen and Altunkaynak 2003) as

$$\hat{K}x = \frac{\sum_{i=1}^{6} K_{xi}A_i}{\sum_{i=1}^{6} A_i} = \frac{0.6\times 34 + 10.8\times 63 + 10\times 115 + 15\times 123.3 + 32\times 160 + 32\times 206.7}{0.6 + 10.8 + 10 + 15 + 32 + 32} = 153.7\,\mathrm{m}^2/\mathrm{s}. \quad (11)$$

Note that K_{xi} in Equation (11) stands for the centroid value of the dispersion coefficient in subarea A_i as shown in Figure 8 and $\hat{K}x$ stands for the crisp output value as a result of centroid defuzzification of the combined fuzzy inference set.

The developed fuzzy model was first applied to predict the K_x from Q used for constructing the fuzzy model (calibration set). Figure 9(a) shows the fuzzy-model-predicted K_x versus measured K_x for the calibration set. For this calibration run $R^2 = 0.83$ and $MAE = 32.1\,\mathrm{m}^2/\mathrm{s}$. Figure 9(a) also shows a band width with $\mp 2SE$ about the regression line, where the computed SE is $55.8\,\mathrm{m}^2/\mathrm{s}$. As seen in Figure 9(a), there are only 3 points (out of 63) outside the band width. In other words, band width accounts for about 95% of the scatter points. These results imply the successful calibration of the fuzzy model.

Table 3 Constructed fuzzy rules (*V*: very; *L*: kow; *M*: medium; *H*: high)

Rule no.	Rules			
1	**IF**	Q is *VVL*	**THEN**	K_x is *VVL*
2	**IF**	Q is *VL*	**THEN**	K_x is *VL*
3	**IF**	Q is *L*	**THEN**	K_x is *L*
4	**IF**	Q is *M*	**THEN**	K_x is *M*
5	**IF**	Q is *H*	**THEN**	K_x is *H*
6	**IF**	Q is *VH*	**THEN**	K_x is *H*
7	**IF**	Q is *VVH*	**THEN**	K_x is *VVH*

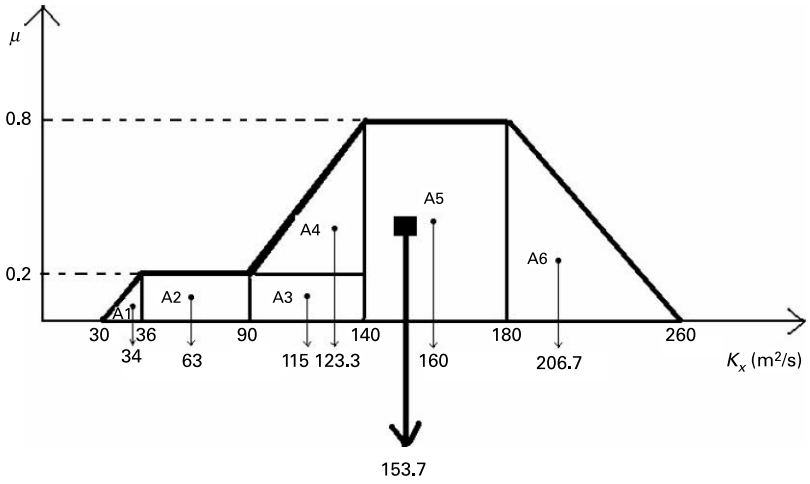

Figure 8 Combined fuzzy output set (inrefence set) for defuzzification

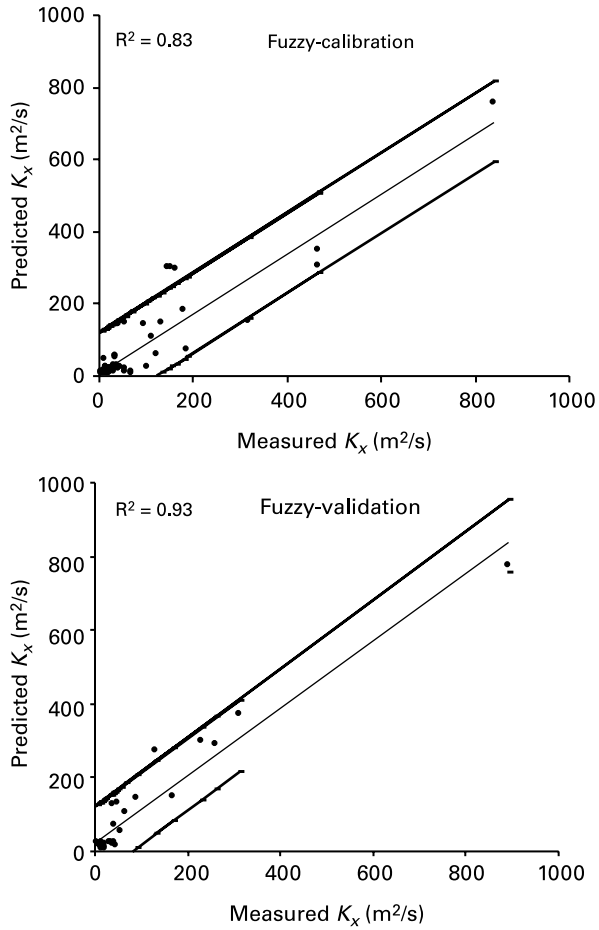

Figure 9 Measured K_x versus fuzzy model-predicted K_x: (a) calibration; (b) validation

The calibrated fuzzy model was then applied to predict the remaining 29 K_x values (validation set marked by * in Table 1). Figure 9(b) presents fuzzy-model-predicted K_x versus measured K_x for the validation set. As seen in Figure 9(b), the model successfully predicted the measured data with $R^2 = 0.93$, $MAE = 31.9\,m^2/s$, and $MRE = 83$. Figure 9(b) also shows the band width about the regression line, where the computed SE is $49.2\,m^2/s$. As seen in Figure 9(b), there is 1 point (out of 63) outside the band width. In other words, band width accounts for 98% of the scatter points. This implies that the developed fuzzy model can predict about 98% of the measured data with $\mp 98.4 m^2/s$.

Note that R^2 values are higher in the validation runs than in the calibration runs for each model. This is because the input data shows a wide variation and the calibration set, naturally, has more values of extreme highs and extreme lows.

Comparative analysis of the results and discussion

The performances of the developed models were qualitatively investigated against each other and against the equations represented by Equations (2), (3), (5), and (6). The comparison of the results are presented in Figure 10 and Table 4. As seen in Figure 10, the newly developed models perform, in general, satisfactorily in predicting low as well as high values of the dispersion coefficient. As seen in Table 4, 12 of the 29 measured data were closely predicted by the fuzzy model, as opposed to 7 by ANN, 5 by Equation (9), 4 by Equation (6), 6 by Equation (5), 3 by Equation (3) and 5 by Equation (2). In other words, the fuzzy model better predicted 41% of the measured data, as opposed to 24% by ANN, 17% by Equation (9), 14% by Equation (6), 21% by Equation (5), 10% by Equation (3) and 17% by

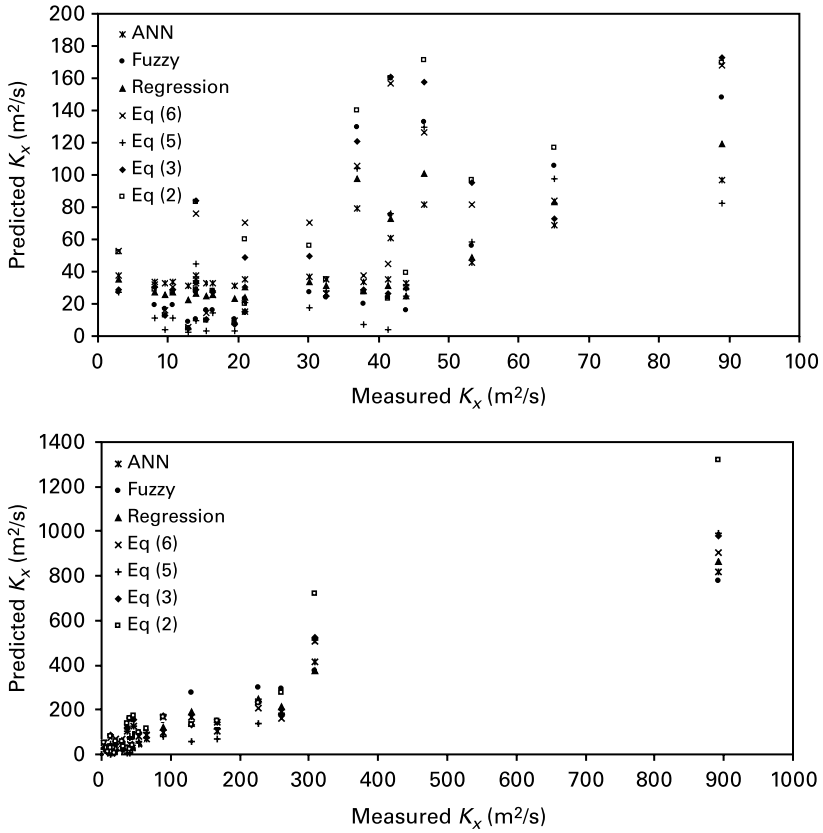

Figure 10 Measured K_x versus predicted K_x

Table 4 Prediction results of measured K_x (m^2/s) data by the models

River	Measured	Fuzzy	ANN	Eq (9)	Eq (6)	Eq (5)	Eq (3)	Eq (2)
Antietam Creek, MD	**20.9**	11.8	29.7	24.4	15.4	15.2	15.3	***20.2***
Monocacy River, MD	**37.8**	17.2	31.6	27.7	***38.0***	7.6	29.0	27.2
Monocacy River, MD	**41.4**	22.3	33.6	30.9	***44.6***	4.2	26.6	23.6
Conococheague Creek, MD	**53.3**	***48.7***	45.1	***49.0***	81.3	58.7	95.5	96.8
Cattahoochee River, GA	**88.9**	149.0	100.7	119.6	167.8	***82.1***	173.0	169.3
Bear Creek, CO	**2.9**	***27.0***	36.0	34.9	53.0	***27.1***	28.7	52.3
Tangipahoa River, LA	**44.0**	12.8	30.1	25.1	30.5	24.5	29.5	***39.3***
Sabina River, LA	**308.9**	***350.0***	427.2	376.2	509.8	512.2	522.4	719.3
Sabina River, TX	**12.8**	***8.0***	28.4	22.2	5.5	2.4	4.7	5.2
Wind/Big River, WY	**41.8**	75.4	***62.3***	73.2	156.8	75.9	160.7	160.0
Clinch River, VA	**10.7**	15.8	31.1	26.9	30.1	***11.5***	29.2	27.6
Clinch River, VA	**36.9**	122.0	***81.5***	97.6	105.3	104.1	121.0	139.7
Powell River, TN	**15.5**	***13.0***	30.1	25.2	***14.4***	2.9	10.1	9.9
John Day River, OR	**13.9**	***26.7***	35.8	34.6	75.8	44.8	83.8	83.3
John Day River, OR	**65.0**	94.3	***70.3***	83.6	83.9	97.9	72.6	116.8
White River	**30.2**	***26.1***	***35.4***	***33.9***	70.4	17.4	49.8	55.8
Missouri River	**892.0**	799	847.3	***865.1***	***904.2***	990.3	976.9	1318.4
Copper Creek, VA	**19.5**	9.1	28.7	***22.9***	10.0	2.9	7.3	8.0
Clinch River, TN	**46.5**	127.0	***84.1***	100.6	126.3	129.3	157.7	171.3
Powell River, TN	**9.5**	13.6	30.3	25.5	16.2	4.2	***12.7***	***12.5***
Clinch River, VA	**8.1**	16.1	31.2	27.0	32.4	***11.3***	30.1	28.9
Antietam Creek	**16.3**	***13.3***	30.2	25.4	25.5	***14.8***	27.9	27.7
Monocacy River	**13.9**	***14.6***	30.7	26.2	35.1	9.6	29.0	28.6
Elkhorn River	**20.9**	***21.3***	33.1	30.3	70.2	***20.5***	48.6	60.0
Muddy Creek	**32.5**	22.2	***33.5***	***30.9***	26.3	27.7	24.9	35.4
Cattahoochee River, GA	**166.9**	***152.0***	102.7	127.0	143.4	68.8	146.6	148.0
Red River, LA	**130.5**	274.0	161.7	189.5	140.5	58.8	***134.4***	***132.9***
Red River, LA	**227.6**	302.0	***238.5***	248.8	205.7	137.8	***238.1***	230.0
Yadkin River, NC	**260.1**	***291.0***	190.5	210.8	163.2	183.7	177.2	***277.0***

Equation (2). In order to objectively evaluate the model performances, the most commonly used error measures of mean absolute error (*MAE*), mean relative error (*MRE*) and discrepancy ratio (*DR*) were evaluated for each model. Table 5 shows the computed *MAE* and *MRE* values. As seen in Table 5, the newly developed models have the lowest *MAE* and *MRE* values. The fuzzy and the regression-based (Equation (9)) models have the minimum $MRE = 0.83$ and $MAE = 23.1\,m^2/s$ values, respectively (Table 5). The Equation (2) and Equation (6) models have the highest $MAE = 59.0\,m^2/s$ and $MRE = 2.36$ values, respectively (Table 5).

The computed $DR = \log(K_{xp}/K_{xm})$ values were presented in Figure 11. Note that if $DR = 0.0$, then there is an exact prediction ($K_{xp} = K_{xm}$). Otherwise, there is either an over-prediction ($DR > 0.0$; $K_{xp} > K_{xm}$) or under-prediction ($DR < 0.0$; $K_{xp} < K_{xm}$). Table 6 summarizes the mean and standard deviation values of computed *DR* values presented in Figure 11 for each model. According to Figure 11, the *DR* distribution of the developed models are similar, showing almost symmetrical distribution between $-0.3 < DR < 1.0$. That is, there is a slight skewness towards the positive zone, implying that the models slightly overestimated the measured data. This is also seen in Table 6 that shows that 68% of the *DR* values fall between -0.19–0.48 and 95% of the values are between -0.47–0.76. The model developed by Kashefipour and Falconer (2002) (Equation (5)) shows significant skewness towards the negative zone, implying that their model underestimated the measured data. This is also seen in Table 6 that shows that 68% of the computed DR values for this model fall between -0.53–0.31 and 95% of the values are between -0.95–0.73. The accuracy of each model may be categorized by the number of *DR* values between -0.3 and 0.3 relative to the total number of data values (Kashefipour and Falconer 2002). Table 5

Table 5 *MAE* (m^2/s), *MRE* and *Accuracy* for each model (*MAE*: mean absolute error; *MRE*: mean relative error; *Accuracy*: the number of *DR* (discrepancy ratio) values between -0.3 and 0.3 relative to the total number of data values)

	Fuzzy	ANN	Eq (9)	Eq (6)	Eq (5)	Eq (3)	Eq (2)
MAE	31.9	25.7	23.1	37.4	37.5	39.8	59.0
MRE	0.83	1.14	0.97	2.36	1.29	1.25	1.60
Accuracy (%)	79	70	76	62	59	62	59

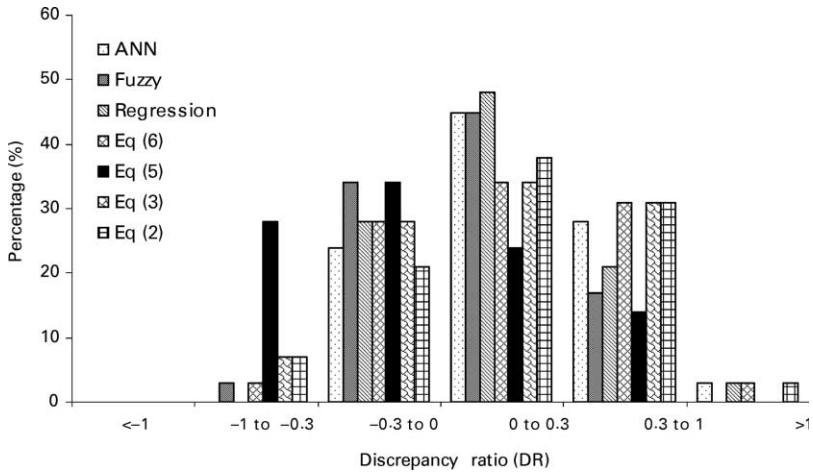

Figure 11 Comparison of discrepancy ratio (*DR*) values for each model

Table 6 Mean (m) and standard deviation (s) of DR (discrepancy ratio) for each model

	Fuzzy	ANN	Eq (9)	Eq (6)	Eq (5)	Eq (3)	Eq (2)
m	0.09	0.20	0.17	0.20	0.11	0.16	0.21
s	0.28	0.28	0.26	0.35	0.42	0.35	0.36
$m \mp s$	−0.19–0.37	−0.08–0.48	−0.09–0.43	−0.15–0.55	−0.53–0.31	−0.19–0.51	−0.15–0.57
$m \mp 2s$	−0.47–0.65	−0.36–0.76	−0.35–0.69	−0.50–0.90	−0.95–0.73	−0.54–0.86	−0.51–0.93

gives the accuracy of each model. As seen in Table 5, the accuracy of the fuzzy model is 79%, which is the highest of all. The fuzzy model is followed by the regression-based model (Equation (9)) and ANN models with 76% and 70% accuracy, respectively. The existing equations (Equations (2), (3), (5), and (6)) showed similar performances with respect to the accuracy rates around 60% (Table 5). The above qualitative results imply that the newly developed regression-based and artificial intelligence models of ANN and fuzzy have superiority over the existing models and they can be employed for predictive purposes.

Summary and conclusions

The existing empirical and theoretical equations express K_x as a function of channel geometric and flow characteristics parameters (U, u_*, H, B, B/H, U/u_*). The scatter diagrams of the field data along with the R^2 values revealed that there is not a strong dependence between each parameter and K_x. These models perform differently for the same flow and channel conditions. This study developed alternative models that would have general applicability.

The scatter diagram of the data revealed that there is a strong dependence between flow discharge (Q) and K_x. Hence, this study proposed to predict K_x from Q by linear regression, ANN, and fuzzy models. For this purpose, a total of 92 sets of K_x–Q data from 30 natural streams were employed. The data were separated into two groups as calibration and validation sets. The 63-calibration data set was used for constructing and calibrating the regression-based and fuzzy models and training the ANN model. The 29-validation data set was used for verifying each developed model.

The performances of the developed models were tested against the measured data and those of the existing equations. The results revealed that the newly developed models predicted the measured data satisfactorily with minimum error values and maximum accuracy rates. When the newly developed models are compared against each other, it is seen from the results that all have similar performances although the fuzzy model has the highest accuracy rate.

Thus the models developed in this study are proposed to be alternatives to the existing equations for predicting the dispersion coefficient in natural streams.

References

Abebe, A.J., Solomatine, D.P. and Venneker, R.G.W. (2000). Application of adaptive fuzzy rule-based models for reconstruction of missing precipitation events. *Hydrol. Sci. J., IAHS*, **45**(3), 425–436.

ASCE (2000). Artificial neural networks in hydrology. I: Preliminary concepts. *J. Hydrol. Engng., ASCE*, **5**(2), 115–123.

Bardossy, A. and Dissi, M. (1993). Fuzzy rule-based models for infiltration. *Wat. Res. Res.*, **29**(2), 373–382.

Bardossy, A. and Duckstein, L. (1995). *Fuzzy Rule-based Modelling With Applications to Geophysical, Biological and Engineering Systems*, CRC Press, New York.

Chang, H.H. (1988). *Fluvial Processes in River Engineering*, Wiley, New York, pp. 10–27, 306–309.

Chuntian, C. (1999). Fuzzy optimal model for the flood control system of the upper and middle reaches of the Yangtze River. *Hydrol. Sci. J., IAHS*, **44**(4), 573–582.

Coppala, E., Duckstein, L. and Davis, D. (2002). Fuzzy rule-based methodology for estimating monthly groundwater recharge in temperate watershed. *J. Hydrol. Engng., ASCE*, **7**(4), 326–335.

Deng, Z.Q., Bengtsson, L., Singh, V.P. and Adrian, D.D. (2002). Longitudianl dispersion coefficient in single-channel streams. *J. Hydraul. Engng., ASCE*, **128**(10), 901–916.

Deng, Z.Q., Singh, V.P. and Bengtsson, L. (2001). Longitudinal dispersion coefficient in straight rivers. *J. Hydraul. Engng., ASCE*, **127**(11), 919–926.

Dou, C., Woldt, W. and Bogardi, I. (1999). Fuzzy rule-based approach to describe solute transport in the unsaturated zone. *J. Hydrol.*, **220**(1–2), 74–85.

Dou, C., Woldt, W., Bogardi, I. and Dahab, M. (1997). Numerical solute transport simulation using fuzzy set approach. *J. Contaminant Hydrol.*, **27**(1–2), 107–126.

Elder, J.W. (1959). The dispersion of a marked fluid in turbulent shear flow. *J. Fluid Mech.*, **5**(4), 544–560.

Fischer, H.B., List, E.J., Koh, R.C.Y., Imberger, J. and Brooks, N.H. (1979). *Mixing in Inland and Coastal Waters*. Academic, New York, pp. 104–138.

Hundecha, Y., Bardossy, A. and Theisen, H.W. (2001). Development of a fuzzy logic-based rainfall-runoff model. *Hydrol. Sci. J., IAHS*, **46**(3), 363–376.

Jantzen, J. (1999). Design of fuzzy controllers. *Technical Report* **98**-E864. Department of Automation, Technical University of Denmark.

Kashefipour, M.S. and Falconer, R.A. (2002). Longitudinal dispersion coefficients in natural channels. *Wat. Res.*, **36**(6), 1596–1608.

Kosko, B. (1992). *Fuzzy Thinking: The New Science of Fuzzy Logic*. Hyperion, New York.

Lu, R-S. and Lo, S-L. (2002). Diagnosing reservoir water quality using self-organizing maps and fuzzy theory. *Wat. Res.*, **36**(9), 2265–2274.

McNeill, F.M. and Thro, E. (1994). *Fuzzy Logic: A Practical Approach*. Hyperion, New York.

McQuivery, R.S. and Keefer, T.N. (1976). Convective model of longitudinal dispersion. *J. Hydraul. Div., ASCE*, **102**(10), 1409–1424.

Ozelkan, E.C. and Duckstein, L. (2001). Fuzzy conceptual rainfall-runoff models. *J. Hydrol.*, **253**(1–4), 41–68.

Ozelkan, E.C., Ni, F. and Duckstein, L. (1996). Relationship between monthly atmospheric circulation patterns and precipitation: fuzzy logic and regression approaches. *Wat. Res. Res.*, **32**(7), 2097–2103.

Raj, A.P. and Kumar, D.N. (1998). Ranking multi-criterion river basin planning alternatives using fuzzy members. *Fuzzy Sets Syst.*, **100**(1–3), 89–99.

Rochusaar, L. and Paal, L. (1970). The results of the experimental investigation of the longitudinal dispersion coefficient in open channels. *Proc. Tallin Politech Inst. A* **298**(6).

Rowinski, P.M., Piotrowski, A. and Napiorkowski, J.J. (2005). Are artificial neural network techniques relevant for the estimation of longitudinal dispersion coefficient in rivers? *Hydrol. Sci. J.*, **50**(1), 175–187.

Sen, Z. (1998). Fuzzy algorithm for estimation of solar irradiation from sunshine duration. *Solar Energy*, **63**(1), 39–49.

Sen, Z. (1999). Fuzzy modeling in engineering. *Class Notes*, Civil Engineering Faculty, Istanbul Technical University, Istanbul, Turkey (in Turkish).

Sen, Z. and Altunkaynak, A. (2003). Fuzzy awakening in rainfall-runoff modeling. *Nord. Hydrol.*, **35**(1), 31–43.

Seo, I.W. and Cheong, T.S. (1998). Predicting longitudinal dispersion coefficient in natural streams. *J. Hydraul. Engng., ASCE*, **124**(1), 25–32.

Sooky, A.A. (1969). Longitudinal dispersion in open channels. *J. Hydraul. Engng., ASCE*, **95**(4), 1327–1346.

Sukhodolov, A.N., Nikora, V.I., Rowinski, P.M. and Czernuszenko, W. (1997). A case study of longitudinal dispersion in small lowland rivers. *Wat. Environ. Res.*, **69**(7), 1246–1333.

Tayfur, G. (2002). Artificial neural networks for sheet sediment transport. *Hydrol. Sci. J.*, **47**(6), 879–892.

Tayfur, G., Ozdemir, S. and Singh, V.P. (2003). Fuzzy logic algorithm for runoff-induced sediment transport from bare soil surfaces. *Adv. Wat. Res.*, **26**, 1249–1256.

Tayfur, G. and Singh, V.P. (2005). Predicting longitudinal dispersion coefficient in natural streams by artificial neural network. *J. Hydraul. Engng., ASCE*, **131**(11), 991–1000.

Tayfur, G., Swiatek, D., Wita, A. and Singh, V.P. (2005). Case study: finite element method and artificial neural network models for flow through Jeziorsko earthfill dam in Poland. *J. Hydraul. Engng., ASCE*, **131**(6), 431–440.

Taylor, G.I. (1953). Dispersion of soluble matter in solvent flowing slowly through a tube. *Proc. Royal Soc. London, Ser. A*, **219**, 186–203.

Taylor, G.I. (1954). The dispersion of matter in turbulent flow through a pipe. *Proc. Royal Soc., London, Ser. A*, **223**, 446–468.

Toprak, Z.F., Sen, Z. and Savci, M.E. (2004). Comment on "Longitudinal dispersion coefficients in natural channels". *Wat. Res.*, **38**, 3139–3143.

Zadeh, L. and Kacprzyk, J. (Eds.)(1992). *Fuzzy Logic for the Management of Uncertainty*. Wiley, New York.